J. Fluid Mech. (1991), *vol.* 227, *pp.* 135–160
Printed in Great Britain

Wave forces on three-dimensional floating bodies with small forward speed

By JAN NOSSEN, JOHN GRUE AND ENOK PALM
Department of Mathematics, University of Oslo, Norway

(Received 19 June 1990 and in revised form 5 November 1990)

A boundary-integral method is developed for computing first-order and mean second-order wave forces on floating bodies with small forward speed in three dimensions. The method is based on applying Green's theorem and linearizing the Green function and velocity potential in the forward speed. The velocity potential on the wetted body surface is then given as the solution of two sets of integral equations with unknowns only on the body. The equations contain no water-line integral, and the free-surface integral decays rapidly. The Timman–Newman symmetry relations for the added mass and damping coefficients are extended to the case when the double-body flow around the body is included in the free-surface condition. The linear wave exciting forces are found both by pressure integration and by a generalized far-field form of the Haskind relations. The mean drift force is found by far-field analysis. All the derivations are made for an arbitrary wave heading. A boundary-element program utilizing the new method has been developed. Numerical results and convergence tests are presented for several body geometries. It is found that the wave exciting forces and the mean drift forces are most influenced by a small forward speed. Values of the wave drift damping coefficient are computed. It is found that interference phenomena may lead to negative wave drift damping for bodies of complicated shape.

1. Introduction

An important problem in offshore technology is the slow drift motions of floating marine structures, such as moored ships and oil platforms. The motion is generated by resonance between the moored structures and slowly oscillating nonlinear wave forces, and may have very large horizontal excursions. The ordinary damping mechanisms, due to viscous effects and wave radiation, are often small. In many sea states the so-called wave drift damping is of the same order of magnitude as the viscous forces, and may even be the dominant damping effect. It is therefore of great importance to be able to predict this quantity. Wave drift damping is defined as the increase in the wave drift force due to a small forward velocity for a body moving in waves. By a Taylor expansion of the wave drift force, neglecting higher-order terms, the wave drift damping is proportional to the forward velocity U. The wave drift damping therefore behaves formally as an ordinary linear damping, provided that the increase with U is positive. Usually this is the case. However, in some special examples, as we shall see, the wave drift damping may be negative, and hence destabilize the oscillating system. The concept of wave drift damping appears to have been initially introduced by Wichers & Sluijs (1979) in connection with their free decaying model tests of large-amplitude low-frequency motions, and have been discussed further by Wichers & Huijsmans (1984).

In this paper we present a method to compute first-order unsteady forces and wave drift forces for arbitrary bodies at forward speed in the three-dimensional case. Knowing the wave drift force for small forward speed, the wave drift damping is easily found. We shall show that even a small forward speed has a great impact on the magnitude of the wave drift forces and exciting forces. The forward velocity U is in non-dimensional form given either as a Froude number or by $\tau \equiv U\sigma/g$, where σ is the frequency of encounter and g the acceleration due to gravity. Typical values for the wave period and U in offshore problems are 10 s and 1 m/s, respectively. This gives that $\tau \approx 0.06$. We shall therefore throughout the paper assume that τ is small and only retain linear terms in τ. We also assume that the Froude number is small. These assumptions will lead to essential simplifications in the solution of the boundary-value problem and in the numerical code. Also, this small forward speed assumption means that only ring wave systems are generated due to the presence of the body. Short ship wave systems are disregarded in this approximation.

During the progress of this work Zhao *et al.* (1988) and Zhao & Faltinsen (1989) have published two papers of particular relevance to the present contribution. Their method is very different from ours. They use a hybrid method, where close to the body a boundary-element method with Rankine sources is applied. This region is matched to an outer regime where a multipole expansion is used. We shall, where it is natural, compare the results of their method with ours, and we shall generally find a good agreement.

Very recently another relevant paper has been published by Wu & Eatock-Taylor (1990). They obtain formulae equivalent to our formulae (53) and (54), which are an extension of the Timman–Newman relations. The methods used are not the same. The essential difference is that we, unlike Wu & Eatock-Taylor (1990), in the proof do not develop the velocity potential in a series in τ over the whole free surface, since it is not obvious that such a series converges at large distance from the body. The examples in their paper are all two-dimensional.

In our approach viscous forces are neglected. The fluid flow is assumed irrotational and the fluid incompressible, so potential theory can be used. The boundary conditions are linearized with respect to the incident wave amplitude. Since the Froude number is small, a rigid wall condition applies on the free surface in the steady problem. It is essential that we use a boundary-element method with a Green function satisfying the correct radiation condition at infinity. The solution is expressed as an integral over the wetted body surface and the free surface. We do not need to discretize any control surface far away from the body, as is necessary with methods using a Rankine source as the fundamental solution. Also, we obtain that the contribution from the free surface decays rapidly with increasing distance from the body, and is thus easy to handle numerically. We will also show that applying the correct boundary condition on the body in the steady problem eliminates the usual waterline integral, at least for wall-sided bodies.

To solve the integral equation efficiently, the velocity potential is expanded in an asymptotic series in powers of τ, retaining linear terms. When we calculate the potential far away from the body, we return to the unperturbed integral equations. On expanding the velocity potential in powers of τ, the free-surface integral, which is of higher order in τ, disappears as an unknown in the integral equation. Thus, unknowns are only needed on the wetted body surface. We have also found it appropriate to follow the idea of Huijsmans & Hermans (1985) and expand the Green function in power series of τ, retaining linear terms. Hereby the actual Green

function can be expressed by the Green function for $\tau = 0$, and its derivatives, for which effective subroutines exist.

A special numerical problem arises if the body has sharp edges. The boundary condition is ill-posed at sharp edges and corners, and the resulting boundary integrals are not integrable. This is circumvented by rewriting the integral equations using a special variety of Stokes theorem, known as Tuck's theorem (Ogilvie & Tuck 1969). This reduces the order of the derivatives in the body boundary condition by one, making the boundary integrals singular but integrable.

Numerical examples are presented for several different body geometries and ranges of parameters, and with convergence tests. Also, an analytical extension of the well-known Timman–Newman symmetry relations for the added mass and damping coefficients is presented. It is shown that this relation also holds without neglecting the steady double-body flow around the body in the free surface-condition, which has been done in previous theories (Timman & Newman 1962). Also a far-field form of the Haskind relations with forward speed is derived. Both these analytical formulae are confirmed numerically.

In §2, the mathematical formulation, the Green function and the far-field behaviour of the outgoing waves are discussed. In §3, we describe briefly the numerical solution procedure. The first- and second-order forces are discussed in §§4 and 5, respectively. In §6 we discuss the energy equation and numerical convergence, and §7 is a conclusion of the work.

2. Mathematical formulation

2.1. *The boundary-value problem*

We consider a body B moving horizontally with constant forward speed U and responding to long-crested incoming regular waves with small amplitude A. Let us introduce a reference frame (x, y, z) moving in the same direction as the body with forward speed U, with the undisturbed free surface in the (x, y)-plane, the x-axis in the direction of forward motion, and the z-axis vertically upwards. In this reference frame the body is performing small oscillations due to the incoming waves, while embedded in a uniform current with speed U along the negative x-axis. This configuration is shown in figure 1. We assume the fluid to be homogeneous, incompressible, and of infinite extent in the lower half-space. Viscosity and surface tension are neglected, thus the motion is irrotational. Then there exists a velocity potential Φ for the velocity $\boldsymbol{v} = \nabla\Phi$ that satisfies the Laplace equation

$$\nabla^2\Phi = 0. \tag{1}$$

To first order in the wave amplitude, the velocity potential may be written

$$\Phi = \phi_s(\boldsymbol{x}) + \Phi_D(\boldsymbol{x}, t) + \Phi_R(\boldsymbol{x}, t), \tag{2}$$

where ϕ_s is independent of time, and Φ_D and Φ_R are time harmonic with encounter frequency σ. The steady potential ϕ_s may be written

$$\phi_s = U(\chi - x), \tag{3}$$

where $-Ux$ is the ambient uniform current potential and $U\chi$ is the steady disturbance due to the body. Φ_R is the total radiation potential due to the oscillatory motions of the body, which may be written

$$\Phi_R = \mathrm{Re}\left[\mathrm{i}\sigma\, \mathrm{e}^{\mathrm{i}\sigma t} \sum_{j=1}^{6} \xi_j \phi_j(\boldsymbol{x})\right], \tag{4}$$

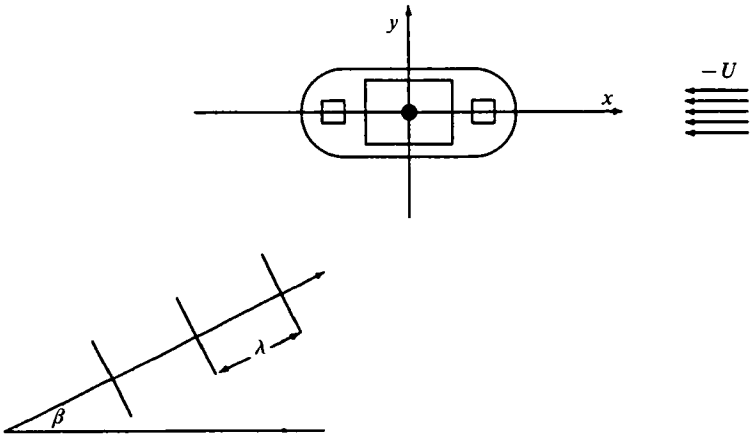

FIGURE 1. Coordinate system with incoming waves and current.

where ξ_j is the amplitude of motion in the jth mode (surge, sway, heave, roll, pitch and yaw, respectively), and ϕ_j is the corresponding radiation potential for unit amplitude of motion. Φ_D is the total diffraction potential, and may be written

$$\Phi_D = \mathrm{Re}\,[A\,e^{i\sigma t}(\phi_0(\boldsymbol{x})+\phi_7(\boldsymbol{x}))], \tag{5}$$

where ϕ_7 is the scattering potential, and ϕ_0 is the potential due to the incoming waves:

$$\phi_0 = \frac{ig}{\omega} e^{Kz} e^{-iK(x\cos\beta+y\sin\beta)}. \tag{6}$$

Here $K = \omega^2/g$ is the zero-speed wavenumber, and ω is the orbital frequency of the incoming wave, given by

$$\omega = \sigma + UK\cos\beta. \tag{7}$$

β is the incidence angle of the incoming waves. The case $\beta = 0$ corresponds to following waves, while $\beta = \pi$ corresponds to head waves.

The steady potential fulfils the body boundary condition

$$\frac{\partial\chi}{\partial n} = n_1 \quad \text{on} \quad S_B \tag{8}$$

corresponding to zero flux through the wetted surface. (n_1, n_2, n_3) denotes the Cartesian components of the normal vector $\boldsymbol{n}$ pointing out of the fluid domain. The body boundary conditions for the unknown potentials ϕ_j, $j = 1, \ldots, 7$, are (Newman 1978)

$$\frac{\partial\phi_j}{\partial n} = \begin{cases} n_j + \dfrac{U}{i\sigma} m_j, & j = 1, \ldots, 6, \\ -\dfrac{\partial\phi_0}{\partial n}, & j = 7, \end{cases} \tag{9}$$

where $(n_4, n_5, n_6) = \boldsymbol{x}\times\boldsymbol{n}$. m_j, $j = 1, 2, 3$ are the components of the vector

$$\boldsymbol{m} = -\boldsymbol{n}\cdot\nabla(\nabla\chi_s) \tag{10}$$

and m_j, $j = 4, 5, 6$ are the components of the vector

$$\boldsymbol{m}' = -\boldsymbol{n}\cdot\boldsymbol{\nabla}(\boldsymbol{x}\times\boldsymbol{\nabla}\chi_s), \tag{11}$$

where

$$\chi_s = \chi - x. \tag{12}$$

Thus, the normal derivative of each radiation potential has two parts. The first, the n-term, represents the oscillatory normal velocity of the body, while the second, the m-term, represents the change in the local steady field due to the motion of the body. Computing the m-terms accurately usually represents a difficult numerical problem. In our case, this will be circumvented by replacing the m-terms in the boundary-integral formulation by first-order derivatives of χ, using a variant of Stokes' theorem known as Tuck's theorem (Ogilvie & Tuck 1969).

Let l be a characteristic dimension of B. If the Froude number $Fr = U/(gl)^{\frac{1}{2}}$ is much less than one, the free-surface condition for the steady potential can be approximated by

$$\frac{\partial\phi_s}{\partial z} = 0 \quad \text{at} \quad z = 0 \tag{13}$$

to first order in the Froude number. The steady problem defined by (8) and (13) can now be easily obtained by a source distribution method. The radiation potentials ϕ_j and the diffraction potential $\phi_D = \phi_0 + \phi_7$ will then satisfy the free-surface condition

$$-\sigma^2\phi_j + 2i\sigma\boldsymbol{\nabla}_1\phi_s\cdot\boldsymbol{\nabla}_1\phi_j + i\sigma\phi_j\nabla_1^2\phi_s + g\frac{\partial\phi_j}{\partial z} = 0 \quad \text{at} \quad z = 0 \tag{14}$$

to the same order. When ϕ_s is precalculated, this is a linear boundary condition with variable coefficients. $\boldsymbol{\nabla}_1$ here means the horizontal gradient. Far away from the body, $\phi_s = -Ux$, and (14) simplifies to the linear boundary condition

$$-\sigma^2\phi_j - 2i\sigma U\frac{\partial\phi_j}{\partial x} + g\frac{\partial\phi_j}{\partial z} = 0 \quad \text{at} \quad z = 0, \tag{15}$$

which only contains known constant coefficients.

Far away from the body, we have a radiation condition stating that ϕ_j, $j = 1, \ldots, 7$, must behave as outgoing waves:

$$\phi_j \sim R^{-\frac{1}{2}}H_j(\theta)\exp\{k_1(\theta)[z - iR(1-4\tau^2\sin^2\theta)^{\frac{1}{2}}]\} \quad \text{as} \quad R\to\infty \tag{16}$$

(see §2.2), where $x = R\cos\theta$, $y = R\sin\theta$. The angle-dependent wavenumber $k_1(\theta)$ is given in the next section by (26). $H_j(\theta)$ are the amplitude distributions of the radiation and scattering potentials.

2.2. *The Green function*

We will solve the radiation and diffraction problems with the boundary condition (14) at the free surface and the boundary conditions (9) on the wetted body surface by applying Green's second identity to the entire fluid domain. As the Green function we will use a pulsating source translating with small forward speed and satisfying the free-surface condition (15). This function is given by

$$G(\boldsymbol{x},\boldsymbol{\xi}) = \frac{1}{r} - \frac{1}{r'} + \Psi(\boldsymbol{x},\boldsymbol{\xi}) \tag{17}$$

with r and r' given by

$$r = [(x-\xi)^2 + (y-\eta)^2 + (z-\zeta)^2]^{\frac{1}{2}} \tag{18}$$

and $$r' = [(x-\xi)^2+(y-\eta)^2+(z+\zeta)^2]^{\frac{1}{2}}, \tag{19}$$

and the wave part of the source potential given by

$$\Psi(x,\xi) = \frac{1}{\pi}\int_0^{2\pi}\int_0^{\infty} \frac{E(\alpha,k)\,\mathrm{d}k\,\mathrm{d}\alpha}{(k-\kappa_1)(1+2\tau\cos\alpha)}, \tag{20}$$

where $$E(\alpha,k) = k\exp[k(z+\zeta)+\mathrm{i}k((x-\xi)\cos\alpha+(y-\eta)\sin\alpha)]. \tag{21}$$

The path of integration is above the pole $k=\kappa_1$ given by

$$\kappa_1(\alpha) = \frac{\nu}{1+2\tau\cos\alpha}, \tag{22}$$

where $\nu = \sigma^2/g$ and $\tau = U\sigma/g$. Later, we will use the far-field behaviour of G. This is obtained by applying contour integration and the method of stationary phase, giving

$$G(R,\theta,z;\xi,\eta,\zeta) = R^{-\frac{1}{2}}h(\xi,\theta)\exp[k_1(\theta)(z+\mathrm{i}R\cos(\alpha_0-\theta))]+O\left(\frac{1}{R}\right), \tag{23}$$

where the stationary phase angle $\alpha_0(\theta)$ is given by

$$\sin(\alpha_0-\theta) = 2\tau\sin\theta, \quad \cos(\alpha_0-\theta) < 0. \tag{24}$$

Thus, we have

$$\cos(\alpha_0-\theta) = -(1-4\tau^2\sin^2\theta)^{\frac{1}{2}}. \tag{25}$$

Furthermore, the wavenumber of the outgoing waves is given by

$$k_1(\theta) = \frac{\nu}{1+2\tau\cos\alpha_0(\theta)}. \tag{26}$$

Hence,

$$G(R,\theta,z;\xi,\eta,\zeta) = R^{-\frac{1}{2}}h(\xi,\theta)\exp\{k_1(\theta)[z-\mathrm{i}R(1-4\tau^2\sin^2\theta)^{\frac{1}{2}}]\}+O\left(\frac{1}{R}\right), \tag{27}$$

where the amplitude $h(\xi,\theta)$ is given by

$$h(\xi,\theta) = \left(\frac{8\pi}{\nu}\right)^{\frac{1}{2}}k_1(\theta)\exp\{k_1(\theta)[\zeta+\mathrm{i}\xi(\cos\theta+2\tau\sin^2\theta) + \mathrm{i}\eta(\sin\theta-2\tau\cos\theta\sin\theta)]-\tfrac{1}{4}\mathrm{i}\pi\}+O(\tau^2). \tag{28}$$

The expressions (27) and (28) are in agreement with the results we obtain from Newman (1959) by assuming that τ is small. They disagree, however, with those of Haskind (1946, eq. 5.21) which do not contain the terms $2\tau\sin^2\theta$ and $2\tau\cos\theta\sin\theta$ in the exponential function in (28). These terms give contributions of order τ which are significant for the forces. Another difference is that the term $4\tau^2\sin^2\theta$ (which is multiplied with R) does not appear in the formula by Haskind. However, this term disappears in the formula for the forces since G is multiplied with G^*.

To first order in τ, α_0 and $k_1(\theta)$ are obtained as

$$\alpha_0 = \pi+\theta-2\tau\sin\theta, \tag{29}$$

$$k_1(\theta) = \nu(1+2\tau\cos\theta). \tag{30}$$

2.3. *Solution of the boundary-value problem*

Let us first consider the diffraction potential. The variable-coefficient condition (14) must be used for ϕ_D on the undisturbed free surface S_F, while the constant-coefficient condition (15) is used for the forward-speed Green function. Let S_∞ denote a vertical

cylinder enclosing the fluid at infinity. We apply Green's theorem to $\phi_D = \phi_0 + \phi_7$ and G, and introduce the boundary condition (9) on the body. This yields

$$\iint_{S_B} \phi_D \frac{\partial G}{\partial n} dS + \iint_{S_F + S_\infty} \left(\phi_D \frac{\partial G}{\partial n} - G \frac{\partial \phi_D}{\partial n} \right) dS = \begin{cases} -4\pi\phi_D(x) \\ -2\pi\phi_D(x), \end{cases} \tag{31}$$

where the first case applies to x in the fluid domain and the second to x on the wetted body surface. (n is pointing out of the fluid.) For the integrals in (31) we apply

$$G(x, \xi; \tau) = G(\xi, x; -\tau). \tag{32}$$

Let C_B denote the waterline curve of the body, and C_∞ the waterline curve of S_∞. Introducing the free-surface conditions (14) for ϕ_D and (15) for G, and applying the two-dimensional divergence theorem, we obtain

$$\iint_{S_F} \left(\phi_D \frac{\partial G}{\partial n} - G \frac{\partial \phi_D}{\partial n} \right) dS = -2i\tau \iint_{S_F} \phi_D (\nabla_1 G \cdot \nabla_1 \chi + \tfrac{1}{2} G \nabla_1^2 \chi) \, dS$$
$$- 2i\tau \int_{C_\infty} \phi_D G \, d\eta + 2i\tau \int_{C_B} \phi_D G \frac{\partial \chi_s}{\partial n} ds. \tag{33}$$

We have assumed that the body is wall-sided at the free surface to obtain the waterline integral on the form above. Applying the boundary condition (8) for χ, we see that the body waterline integral in (33) vanishes exactly. This would not have been the case if we had neglected the steady disturbance χ in the free-surface condition (14).

We now want to eliminate the integral over S_∞ in (31) and the integral over C_∞ in (33). By using the far-field behaviour of the scattering potential, which is given in (16), the far-field behaviour of G, given in (27) and (32), together with Green's theorem for ϕ_0 in the entire fluid domain, we can show that

$$\iint_{S_\infty} \left(\phi_D \frac{\partial G}{\partial n} - G \frac{\partial \phi_D}{\partial n} \right) dS - 2i\tau \int_{C_\infty} \phi_D G \, d\eta + o(\tau) = -4\pi\phi_0 \tag{34}$$

for x in the fluid domain. $o(\tau)$ denotes terms of order smaller than τ.

Introducing (33) and (34) into (31), and omitting $o(\tau)$ terms, we finally obtain

$$\iint_{S_B} \phi_D \frac{\partial G}{\partial n} dS - 2i\tau \iint_{S_F} \phi_D (\nabla_1 G \cdot \nabla_1 \chi + \tfrac{1}{2} G \nabla_1^2 \chi) \, dS - 4\pi\phi_0 = \begin{cases} -4\pi\phi_D(x) \\ -2\pi\phi_D(x), \end{cases} \tag{35}$$

where the first case applies to x in the fluid domain and the second to x on the wetted body surface. We note that (35) include integrals over the body and the free surface.

Using the boundary condition (9) on the body, the corresponding result for the radiation problems can be shown to be

$$\iint_{S_B} \left(\phi_j \frac{\partial G}{\partial n} - G \left(n_j + \frac{U}{i\sigma} m_j \right) \right) dS - 2i\tau \iint_{S_F} \phi_j (\nabla_1 G \cdot \nabla_1 \chi + \tfrac{1}{2} G \nabla_1^2 \chi) \, dS = \begin{cases} -4\pi\phi_j(x) \\ -2\pi\phi_j(x) \end{cases} \tag{36}$$

for $j = 1, \ldots, 6$.

The equations (35) and (36) display some important differences from those usually seen in ship hydrodynamics. In the full linear three-dimensional problem, the steady disturbance χ is usually neglected, leading to integral equations containing a waterline integral. In our case, this integral vanishes because the steady potential $U(\chi - x)$ satisfies the correct boundary condition (8) on the body surface. Instead of

the waterline integral, our equations contain an integral over the free surface. This integral, however, decays very rapidly with increasing distance from the body, since it contains the spatial derivatives of the steady disturbance χ, and χ behaves as a dipole far from the body. Therefore we may always truncate the free surface at a quite short distance from the body.

2.4. *The perturbed equations*

The integral equations (35) and (36) for the unknown potentials ϕ_j and ϕ_D may be simplified by assuming that the reduced frequency $\tau \ll 1$. Expanding ϕ and G in asymptotic series in τ, and keeping only linear terms, we have

$$\phi = \phi^0 + \tau\phi^1, \tag{37}$$

$$G = G^0 + \tau G^1. \tag{38}$$

It must be emphasized that these expansions are local, and only valid at finite distance from the origin.

The right-hand sides in the integral equations for the radiation potentials contain the m-terms, which are given by (10) and (11). These terms are awkward to compute numerically, since they are normal derivatives of the steady velocity. However, the right-hand sides can be rewritten using Tuck's theorem (Ogilvie & Tuck 1969), which states that for any differentiable function f,

$$\iint_{S_B} \nabla\chi_s \cdot \nabla f n_i \,\mathrm{d}S = -\iint_{S_B} f m_i \,\mathrm{d}S - \int_{C_B} f \frac{\partial \chi_s}{\partial z} n_i \,\mathrm{d}s \tag{39}$$

provided that the wetted surface S_B is smooth and that it is wall-sided at the free surface. In our case, the waterline contribution in Tuck's theorem vanishes due to the rigid wall condition (13).

However, the function corresponding to f in the right-hand side of (39) is $G^0(\boldsymbol{x}, \boldsymbol{\xi})$, which is not differentiable at $\boldsymbol{x} = \boldsymbol{\xi}$. This problem may be circumvented by putting $\boldsymbol{x}$ in the fluid and letting it approach the body. Since the right-hand side of (39) (with $f = G^0$) exists when $\boldsymbol{x}$ approaches the body, the left-hand side must also exist in the limit. It follows that the left-hand side of (39) is a principal value integral since $\boldsymbol{n} \cdot \nabla\chi_s = 0$ on the body boundary.

Thus, introducing the asymptotic expansions into (35) and (36), applying Tuck's theorem and collecting terms of the same order in τ, we find the two sets of integral equations:

$$2\pi\phi_j^0 + \iint_{S_B} \phi_j^0 \frac{\partial G^0}{\partial n} \,\mathrm{d}S = \begin{cases} \displaystyle\iint_{S_B} G^0 n_j \,\mathrm{d}S, & j = 1, \ldots, 6 \\ 4\pi\phi_0, & j = \mathrm{D}, \end{cases} \tag{40}$$

$$\begin{aligned} 2\pi\phi_j^1 + \iint_{S_B} \phi_j^1 \frac{\partial G^0}{\partial n} \,\mathrm{d}S &= 2\mathrm{i} \iint_{S_F} \phi_j^0 (\nabla_1 G^0 \cdot \nabla_1 \chi + \tfrac{1}{2} G^0 \nabla_1^2 \chi) \,\mathrm{d}S \\ &\quad - \iint_{S_B} \phi_j^0 \frac{\partial G^1}{\partial n} \,\mathrm{d}S + \begin{cases} \displaystyle\iint_{S_B} \left(G^1 - \frac{1}{\mathrm{i}\nu} \nabla G^0 \cdot \nabla \chi_s \right) n_j \,\mathrm{d}S, & j = 1, \ldots, 6 \\ 0, & j = \mathrm{D} \end{cases} \end{aligned} \tag{41}$$

where $j = \mathrm{D}$ means the diffraction problem. The zero on the right-hand side of the diffraction problem stems from the fact that the incident-wave potential ϕ_0 is independent of τ.

The series expansion simplifies the problem considerably. Since the free-surface integral is of higher order than the other terms, it will only occur at the right-hand side. Thus, when discretizing the equations, we only need to solve for the unknown potentials ϕ^0 and ϕ^1 on the body, not at the free surface.

In addition, the free-surface integral decays very rapidly. Since the steady disturbance χ behaves like a dipole, the integrand decays like R^{-4}, where R is the polar radius. Thus, it is only necessary to discretize the free surface out to 2–3 body diameters.

For a body with sharp edges, Tuck's theorem is not valid. In fact, even the boundary condition (9) is invalid in this case. Equation (9) originates from a Taylor expansion of the boundary condition applied on the moving boundary. This expansion is only valid for smooth surfaces. The result is that the m-terms are not even integrable at an edge. With this reformulation, however, the right-hand side is integrable as long as the field point is not situated directly at the edge. Therefore we believe that this formulation will lead to better numerical behaviour at the edge. An alternative approach for integrating the singular corner flow is given by Zhao & Faltinsen (1989).

3. Numerical methods

3.1. *Solution of the integral equations*

The integral equations (40) and (41) are solved by a conventional panel method. The body is approximated by plane quadrilateral elements, and the velocity potential is assumed constant over each panel. Using the panel centroids as collocation points, the integral equations are reduced to sets of complex linear equations.

To compute the free-surface integral, the free surface is panelized in the same manner as the wetted body surface. However, since this integral only contributes to the right-hand sides of the equations, this means very little additional computer memory usage. The free surface is truncated at about 3 body diameters' distance from the centre of the body.

In all the calculations, the singular terms of the various Green functions are integrated by the Hess and Smith method. The logarithmic singularities have been integrated by the method of Newman & Sclavounos (1987). Numerical integrations over each panel are performed using the mid-point rule, except when we compute the influence of a point on itself, which is done by four-point Gaussian integration. Our program is also designed to use four-point Gaussian quadrature over all panels. Experience shows that this does not improve the results significantly, and the four-point method increases the total CPU time of the computations by a factor of about 2 compared to the mid-point method.

No special algorithms are used to take care of the corner singularities for bodies with sharp corners. However, since the integral formulation (41) is used, the right-hand sides in the radiation problems are integrable. The errors associated with these terms are therefore assumed to be small.

3.2. *The Green function*

The translating pulsating source with small forward speed is given by (17)–(20). Following Huijsmans & Hermans (1985), we now expand the wave part of the source potential, Ψ, in powers of τ:

$$\Psi = \psi_0 + \tau\psi_1 + \dots . \tag{42}$$

This is an asymptotic expansion, which is not uniformly valid. It can be used locally, but not at infinite distance from the source point. ψ_0 is the zero-speed source potential given by

$$\psi_0 = 2\int_0^\infty \frac{k\,\mathrm{e}^{k(z+\zeta)}}{k-\nu} J_0(kR)\,\mathrm{d}k, \tag{43}$$

where $R = [(x-\xi)^2+(y-\eta)^2]^{\frac{1}{2}}$, J_0 is the Bessel function of the first kind and zero order and $\nu = \sigma^2/g$. The first-order correction term can be written as

$$\psi_1 = -4\mathrm{i}\frac{x-\xi}{R}\int_0^\infty \frac{k^2\,\mathrm{e}^{k(z+\zeta)}}{(k-\nu)^2} J_1(kR)\,\mathrm{d}k, \tag{44}$$

where J_1 is the Bessel function of the first kind and first order. We note that

$$\psi_1 = 2\mathrm{i}\frac{\partial^2\psi_0}{\partial\nu\,\partial x}. \tag{45}$$

Thus, the Green function for small forward speed can be expressed by means of the real and imaginary parts of the zero-speed Green function and its derivatives. The integrals of ψ_1 and $\partial\psi_1/\partial n$ in (40) and (41) may be rewritten to involve only $\partial\psi_0/\partial R$, $\partial\psi_0/\partial z$ and $(1/R)\,\partial\psi_0/\partial R$. The major singularities to be integrated are thus $1/r'$, $\ln\nu(r'+|z+\zeta|)$ and their gradients. These singularities are integrated analytically.

4. The first-order wave forces

Having found the velocity potential by the method presented in the previous sections, the first-order wave forces can now be found by pressure integration over the body surface. Here, we will develop some useful formulae for the forces and examine some important properties of the added mass and damping coefficients and the linear exciting force coefficients.

4.1. *Added mass and damping*

The added mass and damping coefficients can now be obtained from the radiation potentials. Denoting the added mass coefficients by a_{ij} and the damping coefficients by b_{ij}, we can express the radiation force and moment by applying the Bernoulli equation, as

$$F_i = \mathrm{Re}\,(-\mathrm{i}\sigma\xi_j\,\mathrm{e}^{\mathrm{i}\sigma t} f_{ij}). \tag{46}$$

Here $i,j = 1,\ldots,6$, and the complex force coefficients f_{ij} are defined as

$$f_{ij} \equiv \mathrm{i}\sigma a_{ij} + b_{ij} = \rho\iint_{S_B} (\mathrm{i}\sigma\phi_j + \nabla\phi_s\cdot\nabla\phi_j)\,n_i\,\mathrm{d}S. \tag{47}$$

Using Tuck's theorem (39), we obtain

$$f_{ij} = \rho\iint_{S_B} (\mathrm{i}\sigma n_i - Um_i)\,\phi_j\,\mathrm{d}S. \tag{48}$$

Timman & Newman (1962) have shown that when the steady disturbance field χ is neglected in the free-surface condition (14), the added mass and damping satisfy the so-called Timman–Newman relations

$$f_{ij}(U) = f_{ji}(-U), \quad i,j = 1,\ldots,6. \tag{49}$$

That is, the hydrodynamic forces are the same when we reverse the forward speed and exchange indices. We will now use (48) to show that these relations are also satisfied for an arbitrary body with the free-surface condition (14), which includes χ. To show this, we introduce the reversed-flow radiation potentials ψ_j, which satisfy the boundary conditions (9) and (14) with the sign of U reversed (but with the same encounter frequency). Using the definition of ψ_j, we can write

$$f_{ij}(U) = \mathrm{i}\sigma\rho \iint_{S_B} \phi_j \frac{\partial \psi_i}{\partial n} \mathrm{d}S. \tag{50}$$

Applying Green's theorem to ϕ_j and ψ_i, we obtain

$$\begin{aligned} f_{ij}(U) - f_{ji}(-U) &= \mathrm{i}\sigma\rho \iint_{S_B} \left(\phi_j \frac{\partial \psi_i}{\partial n} - \psi_i \frac{\partial \phi_j}{\partial n}\right) \mathrm{d}S \\ &= -\mathrm{i}\sigma\rho \iint_{S_F} \left(\phi_j \frac{\partial \psi_i}{\partial n} - \psi_i \frac{\partial \phi_j}{\partial n}\right) \mathrm{d}S - \mathrm{i}\sigma\rho \iint_{S_\infty} \left(\phi_j \frac{\partial \psi_i}{\partial n} - \psi_i \frac{\partial \phi_j}{\partial n}\right) \mathrm{d}S. \end{aligned} \tag{51}$$

Using the free-surface condition (14) and the two-dimensional divergence theorem, the integral over the free surface can be written

$$-\iint_{S_F} \left(\phi_j \frac{\partial \psi_i}{\partial n} - \psi_i \frac{\partial \phi_j}{\partial n}\right) \mathrm{d}S = 2\mathrm{i}\tau \int_{C_B} \phi_j \psi_i \frac{\partial \chi_s}{\partial n} \mathrm{d}s + 2\mathrm{i}\tau \int_{C_\infty} \phi_j \psi_i \mathrm{d}y. \tag{52}$$

Since the body is wall-sided, we obtain from (8) that the waterline integral at the body vanishes.

Let us then consider the integral over S_∞. The far-field behaviour of ϕ_i and ψ_j is given by (16), where τ is replaced by $-\tau$ in ψ_j. Inserting these expressions into the integral over S_∞ and integrating with respect to the vertical coordinate, we obtain a contribution which to leading order in τ cancels the last integral in (52). Thus, to leading order in τ we have generalized the Timman–Newman relations to be valid with the free-surface condition (14) for a body of general shape, i.e.

$$f_{ij}(U) - f_{ji}(-U) = \mathrm{i}\sigma\rho \iint_{S_B} \left(\phi_j \frac{\partial \psi_i}{\partial n} - \psi_i \frac{\partial \phi_j}{\partial n}\right) \mathrm{d}S = 0. \tag{53}$$

An immediate consequence of (49) is that

$$f_{ii}(\tau) = f_{ii}(0) + o(\tau). \tag{54}$$

Thus, to leading order the diagonal added mass and damping coefficients only depend on the current speed through the frequency of encounter. This is confirmed by the numerical results.

Figures 2 and 3 illustrate the validity of the Timman–Newman relations for a half-immersed sphere of radius a at Froude number $Fr = 0.04$ and 0.08 respectively, where $Fr = U/(ga)^{\frac{1}{2}}$. The free surface is discretized out to a radius of $6a$. The added mass and damping coefficients are computed from (47) to avoid the m-term problem. The surge–heave and heave–surge hydrodynamic coefficients are zero at $Fr = 0$, so at small forward speed they are essentially proportional to Fr. The differences

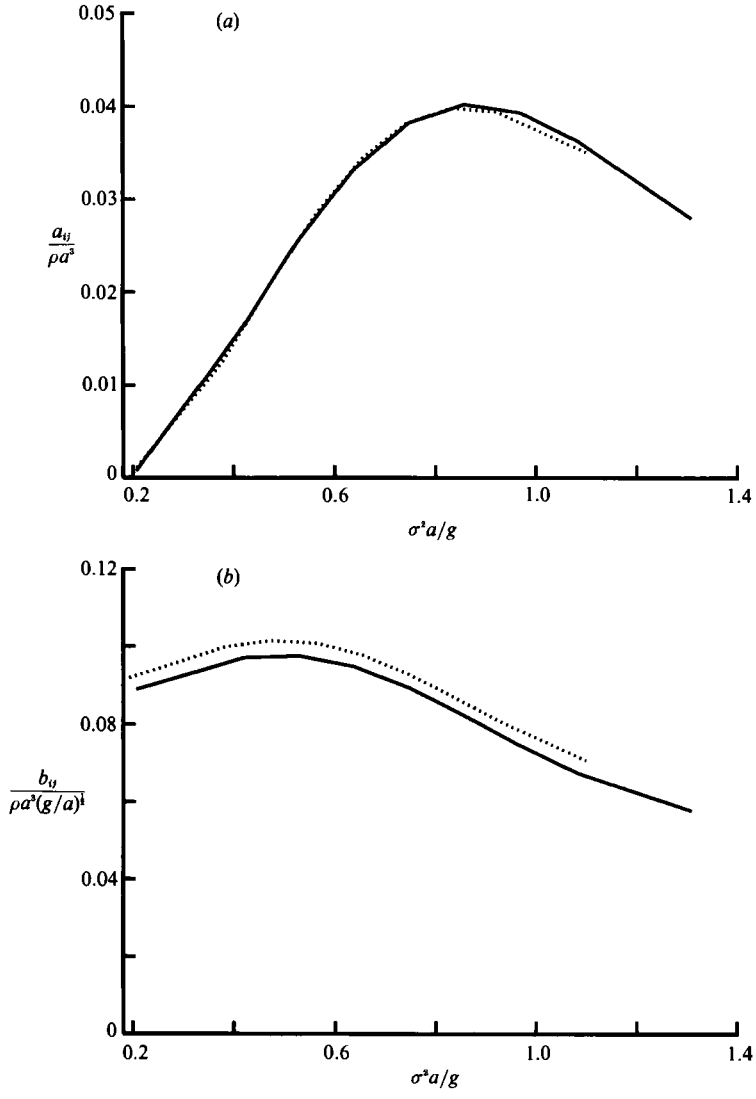

FIGURE 2. Cross-coupling (*a*) added-mass coefficients $a_{13}(U)$ (solid line) *vs.* $a_{31}(-U)$ (dotted line) and (*b*) damping coefficients $b_{13}(U)$ (solid line) *vs.* $b_{31}(-U)$ (dotted line) for a half-immersed sphere of radius a at $Fr = \pm 0.04$. 200 panels on half-S_B, 440 panels on half-S_F.

between the surge–heave and heave–surge coefficients at $Fr = \pm 0.04$ are at most 2% for the added mass and 7% for the damping coefficients. The figures are almost the same for $Fr = \pm 0.08$.

4.2. *The exciting forces*

The Haskind relations express the exciting force in terms of the incident-wave potential ϕ_0 and the reversed-flow radiation potentials ψ_i, so that the first-order exciting forces can be computed without knowing the scattering potential ϕ_7. The Haskind relations for zero forward speed have been known for a long time, see for example Newman (1977). The Haskind relations have been generalized to small forward speed by Zhao & Faltinsen (1988) for the two-dimensional case. Here we derive the Haskind relations with forward speed for the three-dimensional case

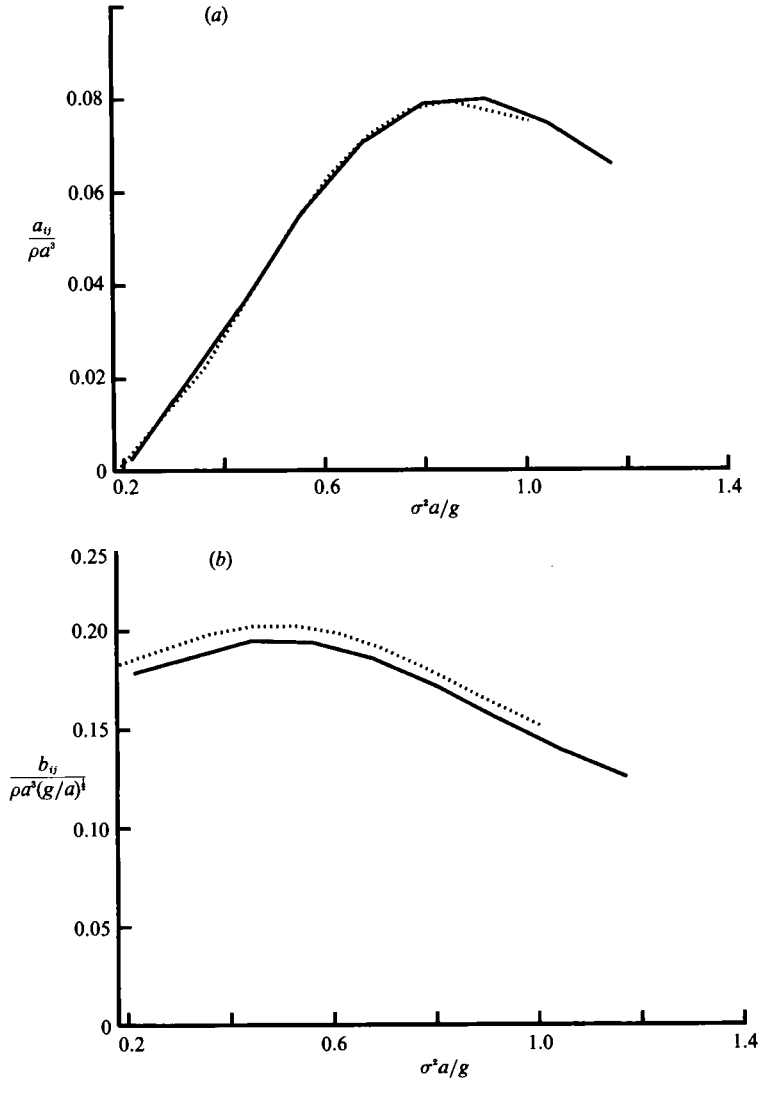

FIGURE 3. Same as figure 2 but $Fr = \pm 0.08$.

expressed by far-field integrals, which then gives the exciting force in a very convenient form. The diffraction force and moment are given as

$$F_i = -\rho \iint_{S_B} \left(\frac{\partial \Phi_D}{\partial t} + \nabla \phi_s \cdot \nabla \Phi_D \right) n_i \, dS, \tag{55}$$

where $i = 1, \ldots, 6$, and Φ_D is the total diffraction potential given by (5). Inserting (5) and applying Tuck's theorem (39), the force and moment may be written

$$F_i = \mathrm{Re}\,(A\, e^{i\sigma t} X_i), \tag{56}$$

where the exciting force coefficients X_i are given as

$$X_i = -i\sigma\rho \iint_{S_B} (\phi_0 + \phi_7) \frac{\partial \psi_i}{\partial n} dS, \tag{57}$$

where ψ_i denotes the reversed-flow radiation potentials. Applying Green's theorem to ϕ_7 and ψ_i, we find that

$$\iint_{S_B+S_F+S_\infty} \left(\phi_7 \frac{\partial \psi_i}{\partial n} - \psi_i \frac{\partial \phi_7}{\partial n}\right) \mathrm{d}S = 0. \tag{58}$$

Using the free-surface condition (14) on $\phi_0+\phi_7$, we have that the free-surface integral can be written

$$\iint_{S_F} \left(\phi_7 \frac{\partial \psi_i}{\partial n} - \psi_i \frac{\partial \phi_7}{\partial n}\right) \mathrm{d}S = 2\mathrm{i}\tau \iint_{S_F} \nabla_1 \cdot (\phi_7 \psi_i \nabla_1 \chi_s)\, \mathrm{d}S$$
$$+ 2\mathrm{i}\tau \iint_{S_F} \psi_i (\nabla_1 \phi_0 \cdot \nabla_1 \chi + \tfrac{1}{2}\phi_0 \nabla_1^2 \chi)\, \mathrm{d}S. \tag{59}$$

The first integral can be rewritten using Gauss' theorem, resulting in a line integral over C_∞ that cancels the surface integral over S_∞, as in the previous chapter. Inserting (59) and the body boundary condition (9) into (58), we obtain

$$\iint_{S_B} \phi_7 \frac{\partial \psi_i}{\partial n} \mathrm{d}S = -\iint_{S_B} \psi_i \frac{\partial \phi_0}{\partial n} \mathrm{d}S - 2\mathrm{i}\tau \iint_{S_F} \psi_i (\nabla_1 \phi_0 \cdot \nabla_1 \chi + \tfrac{1}{2}\phi_0 \nabla_1^2 \chi)\, \mathrm{d}S. \tag{60}$$

Inserting this into equation (57) for the exciting forces, we arrive at the Haskind relations

$$X_i = -\mathrm{i}\sigma\rho \iint_{S_B} \left(\phi_0 \frac{\partial \psi_i}{\partial n} - \psi_i \frac{\partial \phi_0}{\partial n}\right) \mathrm{d}S - 2\sigma\tau\rho \iint_{S_F} \psi_i (\nabla_1 \phi_0 \cdot \nabla_1 \chi + \tfrac{1}{2}\phi_0 \nabla_1^2 \chi)\, \mathrm{d}S. \tag{61}$$

Thus, the exciting forces can be obtained as an integral of the incident-wave potential and the reversed-flow radiation potentials over the body and the free surface. This formula may be rewritten, by applying Green's theorem to ψ_i and ϕ_0, into the alternative form

$$X_i = \mathrm{i}\sigma\rho \iint_{S_\infty} \left(\phi_0 \frac{\partial \psi_i}{\partial n} - \psi_i \frac{\partial \phi_0}{\partial n}\right) \mathrm{d}S + 2\sigma\tau\rho \int_{C_\infty} \phi_0 \psi_i \, \mathrm{d}y. \tag{62}$$

Introducing the far-field expression for ψ_i and applying the method of stationary phase to the integral over θ, we finally obtain

$$X_i = \rho g \left(\frac{2\pi}{K}\right)^{\frac{1}{2}} (1 - 2\tau\cos\beta)\, H_i^-(\beta + \pi + 2\tau\sin\beta)\, \mathrm{e}^{\mathrm{i}\pi/4} + o(\tau), \tag{63}$$

where H_i^- denotes the amplitude distribution of the ith reversed-flow potential, and is obtained from H_i by replacing τ by $-\tau$ (but keeping ν). H_i is found by introducing (16) in (36), which gives

$$H_i(\theta) = -\frac{1}{4\pi} \iint_{S_B} \left(\phi_i \frac{\partial h}{\partial n} - \left(h - \frac{\tau}{\mathrm{i}\nu} \nabla \chi_s \cdot \nabla h\right) n_j\right) \mathrm{d}S$$
$$+ \frac{1}{2\pi} \mathrm{i}\tau \iint_{S_F} \phi_i (\nabla_1 h \cdot \nabla_1 \chi + \tfrac{1}{2} h \nabla_1^2 \chi)\, \mathrm{d}S. \tag{64}$$

The amplitude $h(\xi, \theta)$ of the Green function is given by (28).

Thus, the exciting force with forward speed can be found by evaluating the radiation potential far-field amplitude at one polar angle, just as in the zero-speed case.

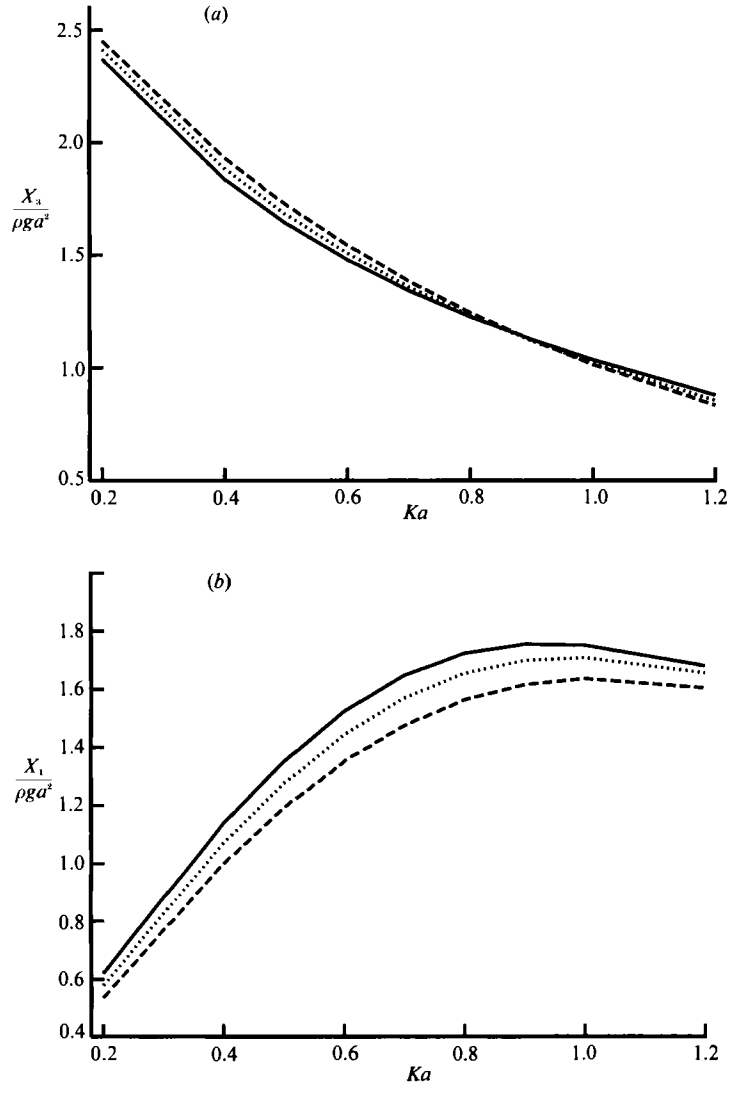

FIGURE 4. (*a*) Heave and (*b*) surge exciting forces for a half-immersed sphere of radius a in head waves. Solid line, $Fr = 0.04$; dotted line, $Fr = 0$; dashed line, $Fr = -0.04$. 200 panels on half-S_B, 440 panels on half-S_F.

Figure 4 shows calculations of the exciting forces for a half-immersed sphere in head waves and $Fr = 0, \pm 0.04$. The far-field Haskind relations (63) are used. We note that the surge exciting force increases with the Froude number for all wavelengths, while the heave exciting force decreases with the Froude number for long waves and increases with the Froude number for short waves.

Figure 5 shows the derivatives of the exciting forces with respect to the forward speed computed by numerical differentiation of the data in figure 4. The method of direct pressure integration is compared to the far-field Haskind relations (63). The agreement between the two methods is excellent.

We observe that the forward speed influence is stronger upon the exciting forces than upon the added mass and damping, and apparently stronger on the surge

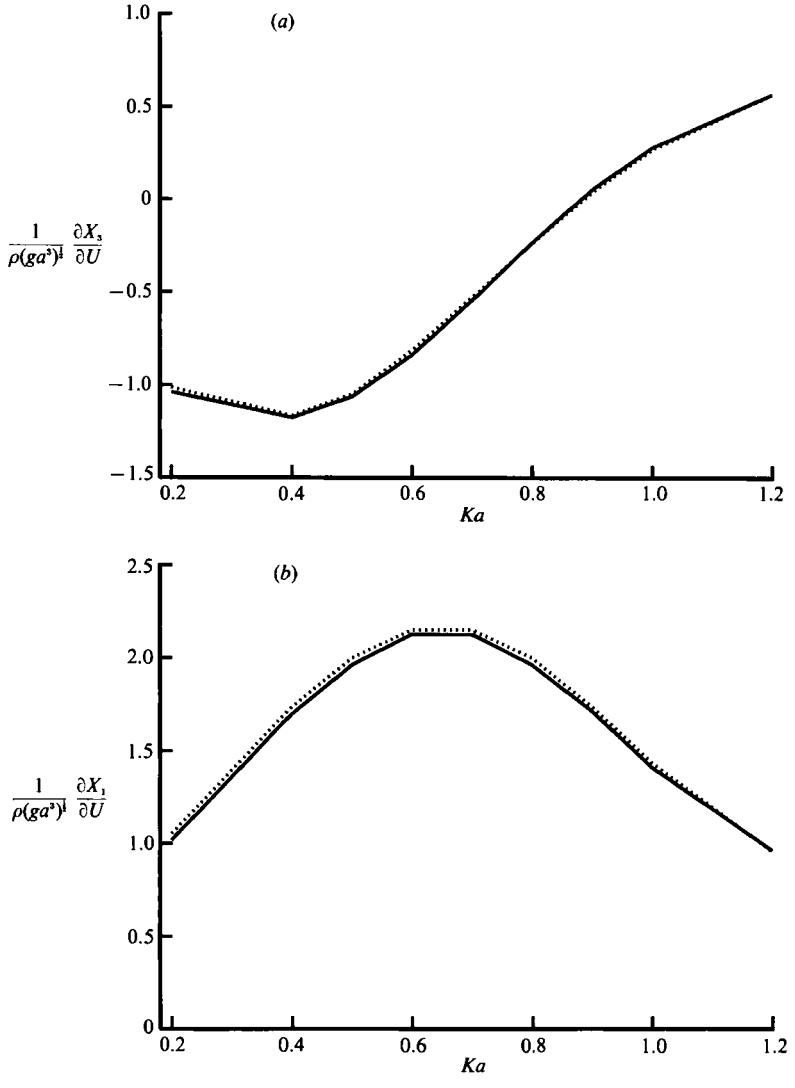

FIGURE 5. Derivative of (*a*) the heave and (*b*) surge exciting forces with respect to U for a half-immersed sphere of radius a in head waves. Comparison of near-field pressure integration (solid line) and far-field Haskind relation (dotted line). 200 panels on half-S_B, 440 panels on half-S_F.

exciting force than the heave force. In the next section, we will see that the influence is even stronger on the drift force.

5. The mean drift force

The mean steady second-order force, the mean drift force, may be computed by direct pressure integration or by using the far-field method. The latter, which is obtained by applying the momentum equation, is most accurate and will be applied here. The mean drift force $\boldsymbol{F}$ is then given by

$$\boldsymbol{F} = -\overline{\iint_{S_\infty} (p\boldsymbol{n} + \rho \boldsymbol{v}\boldsymbol{v}\cdot\boldsymbol{n})\,\mathrm{d}S}, \tag{65}$$

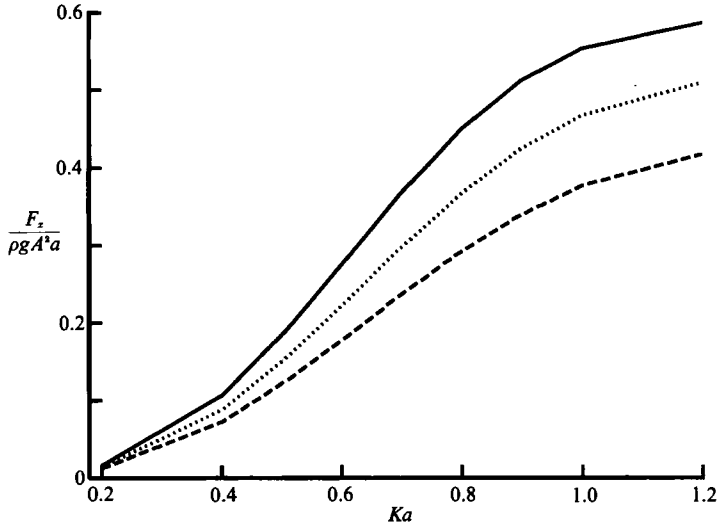

FIGURE 6. Mean drift force on a half-immersed restrained sphere of radius a in head waves. Solid line, $Fr = 0.04$; dotted line, $Fr = 0$; dashed line, $Fr = -0.04$. 200 panels on half-S_B, 440 panels on half-S_F.

where an overbar denotes time-average. Introducing $\boldsymbol{v}' = (u', v', w')$ using $\boldsymbol{v} = -U\boldsymbol{i} + \boldsymbol{v}'$, applying the Bernoulli equation and conservation of mass, it may be shown that (Grue & Palm 1990)

$$\boldsymbol{F} = -\overline{\iint_{S_\infty} (-\rho(\Phi_t + \tfrac{1}{2}|\boldsymbol{v}'|^2 + gz)\,\boldsymbol{n} + \rho \boldsymbol{v}'\boldsymbol{v}'\cdot\boldsymbol{n})\,\mathrm{d}S} + \rho U \overline{\iint_{S_\infty} (\boldsymbol{v}' n_1 - u'\boldsymbol{n})\,\mathrm{d}S}. \tag{66}$$

This expression for the mean force is valid for arbitrary current speed and water depth. We notice that the second term has only a component in the y-direction and is dependent on the velocity circulation. It may be shown that this lift force is of second order in τ. The x-component of (66) was derived by Maruo (1960), assuming infinite water depth. Introducing the velocity potential, we obtain after some calculation for the x-component (i.e. in the current direction)

$$F_x = \rho \int_0^{2\pi} \left\{ -\frac{1}{2g}\left[\overline{\left(\frac{\partial \Phi}{\partial t}\right)^2} - U^2 \overline{\left(\frac{\partial \Phi}{\partial x}\right)^2}\right]_{z=0} \cos\theta + \int_{-\infty}^{0} \left[\tfrac{1}{2}\overline{|\nabla \Phi|^2}\cos\theta - \overline{\frac{\partial \Phi}{\partial x}\frac{\partial \Phi}{\partial R}}\right] \mathrm{d}z \right\} R\,\mathrm{d}\theta. \tag{67}$$

We note that F_x is a function of first-order quantities only, which not generally is true for F_y and the mean yaw moment M_z. We now insert the expressions (6) for ϕ_0 and (16) for the radiation and scattering potentials ϕ_j. Averaging with respect to time and using the method of stationary phase, the wave drift force is obtained as

$$\frac{F_x}{\rho g A^2} = -\frac{1}{4}\left\{ \int_0^{2\pi} B(\theta)\,|H(\theta)|^2\,\mathrm{d}\theta + 2\cos\beta(1 - 2\tau\cos\beta)\,S \right\} + o(\tau), \tag{68}$$

where

$$B(\theta) = (1 - 2\tau\cos\beta)\cos\theta + 2\tau\sin^2\theta,$$

$$S = \left(\frac{2\pi}{\nu}\right)^{\frac{1}{2}} \mathrm{Re}\,(\mathrm{e}^{\mathrm{i}\pi/4} H^*(\beta + 2\tau\sin\beta)), \tag{69}$$

$$\frac{\mathrm{i}g}{\omega} H(\theta) = H_7(\theta) + \mathrm{i}\sigma \sum_{j=1}^{6} \frac{\xi_j}{A} H_j(\theta). \tag{70}$$

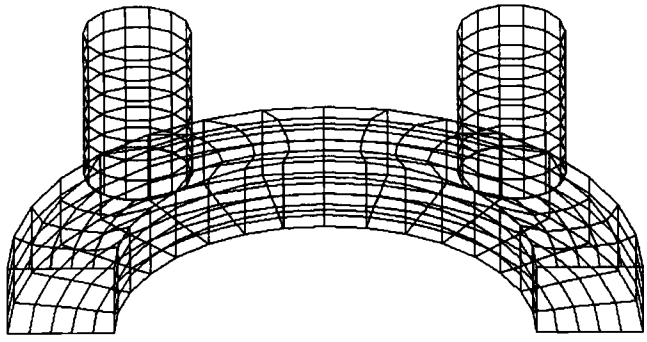

FIGURE 7. The geometry of half an offshore platform.

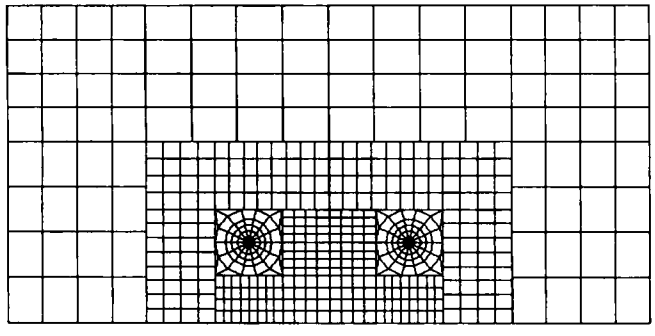

FIGURE 8. Discretization of the free surface around the platform in the half-plane $y > 0$.

A star denotes complex conjugate. $H_j(\theta)$ is given by (64), and $H_7(\theta)$ is given by

$$H_7(\theta) = -\frac{1}{4\pi}\left\{\iint_{S_B} \phi_D \frac{\partial h}{\partial n}\,dS - 2i\tau \iint_{S_F} \phi_D(\nabla_1 h\cdot\nabla_1\chi + \tfrac{1}{2}h\nabla_1^2\chi)\,dS\right\}. \tag{71}$$

Figure 6 shows the mean drift force on a half-immersed sphere in head waves ($\beta = \pi$) at $Fr = 0, \pm 0.04$. The sphere is restrained from moving in first-order motions. As this figure shows, the influence of forward speed is much stronger on the drift force than on the first-order forces.

The forces on an idealized offshore platform are also computed. The submerged part of the platform consists of a horizontal ring-like pontoon carrying four vertical columns. The vertical columns are circular with radius a and height $3a$, and the circular pontoon has a rectangular cross-section, with breadth $2a$ and height $1.4a$. The columns are placed on the pontoon such that their centres form a square with sides $7a$. This configuration is shown in figure 7. Each column is discretized with 98 panels, the half of the pontoon with 288 panels, i.e. the half-body is discretized with a total of 484 panels. On half of the free surface there are 468 panels. The discretization of the free surface is shown in figure 8. The platform is free to surge in linear motion in incoming head waves.

Figure 9 shows the wave drift force for this geometry at zero forward speed. The figure also shows the result when the pontoon is removed. We observe for both bodies typical interference phenomena acting between the different columns. The force is remarkably similar for the platform and the cylinder array, except for the interval

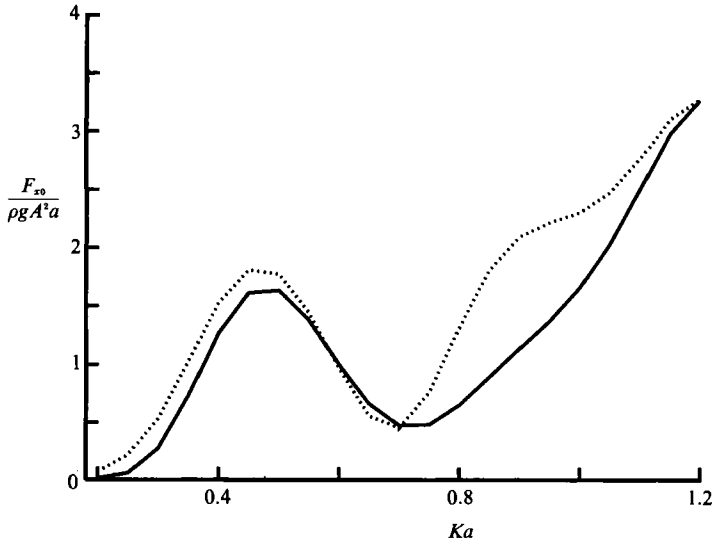

FIGURE 9. Mean drift force on an offshore platform. The platform is free to surge in head waves. $Fr = 0$. Solid line, without pontoon; dotted line, with pontoon.

$0.7 < Ka < 1.0$. For higher frequencies, the pontoon is obviously too deeply submerged to influence the forces. As figure 9 shows, the mean drift force on each cylinder in the array may be considerably greater than the drift force on a single cylinder, which is shown in figure 13 (for small U).

In many practical situations it is of importance to compute the wave drift damping, which is the increase in the mean drift force due to a small current, i.e.

$$F_x = F_{x0} + Fr F_{x1} + o(Fr), \tag{72}$$

where F_{x0} is the mean drift force at zero forward speed and F_{x1} is the wave drift damping coefficient. Figure 10 shows the wave drift damping coefficient for the platform and the cylinder array, as described above. Owing to interference phenomena, the wave drift damping oscillates quite rapidly and even becomes also negative at some frequencies.

For Ka-values close to 0.6 the negative value of wave drift damping is significant and may lead to the result that the sum of viscous damping and wave drift damping becomes small, even negative, for this incident wavenumber. This negative wave drift damping seems to be a result of the wave interference due to the cylinder array. As seen from figures 12 and 14, there is no tendency for negative wave drift damping for a single cylinder.

Comparing figures 9 and 10 it is noted that $\mathrm{d}F_{x0}/\mathrm{d}(Ka)$ has a variation with Ka which is rather similar to the variation of the wave drift damping. It is a rather complex task to find the wave drift damping as displayed in figure 10. A simplified method has therefore been proposed, which assumes that the most important contribution to the wave drift force from the velocity U is the change in frequency, i.e. the Doppler effect. The approximation therefore consists in only considering the mean drift force for $U = 0$, except that in the free-surface condition ω is replaced by σ. The wave drift damping is then obtained by taking the derivative of F_{x0} with respect to σ times $\partial\sigma/\partial U = -K\cos\beta$, or, equivalently, with respect to ω and multiplying with $-K\cos\beta$. Figure 10 also displays the wave drift damping

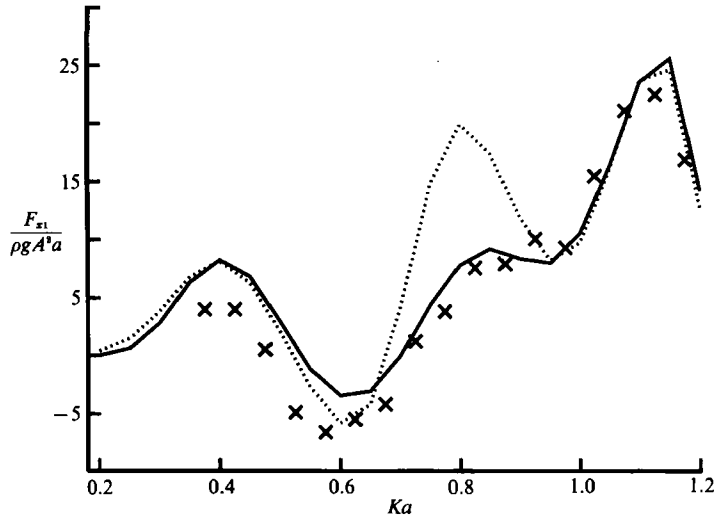

FIGURE 10. Wave drift damping coefficient for an offshore platform obtained by numerical differentiation of F_x at $Fr = \pm 0.005$. The platform is free to surge in head waves. Solid line, without pontoon; dotted line, with pontoon; ×, simplified method for the cylinder array.

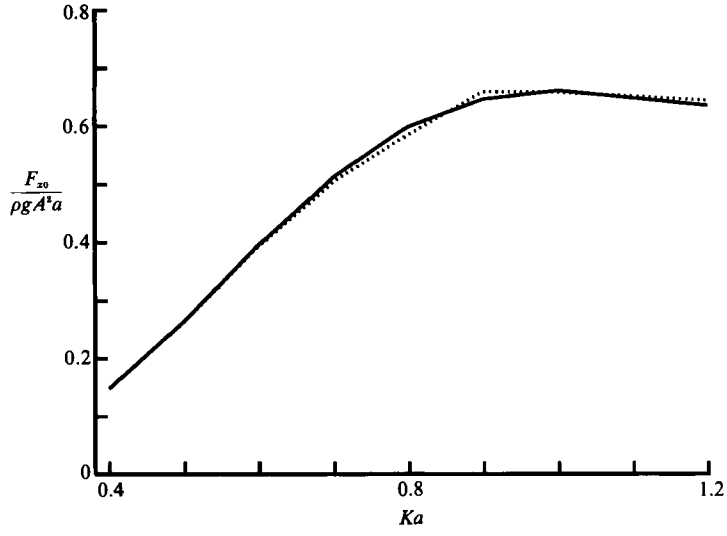

FIGURE 11. Mean drift force on a restrained floating cylinder of radius a and draught $3a$ in head waves. $Fr = 0$. Solid line, present theory, 280 panels on half-S_B, 224 panels on half-S_F; dotted line, Zhao & Faltinsen (1989, figure 15).

coefficient for the cylinder array, as function of Ka, obtained by the simplified method, which often is called the wave drift gradient approach, see for example Schellin & Kirsch (1989). As seen from the figure, this trivial approximation is remarkably good for shorter waves, in this case. The wave drift gradient approach fails completely in many cases, however, see for example figure 11 where $\partial F_{x0}/\partial(Ka) = 0$ for $Ka > 0.8$. $F_{x1}/\rho g A^2 a$ is, however, far from zero in this case.

Values of the wave drift force on a vertical surface-piercing cylinder moving in head waves are shown in figures 11, 12, 13 and 14. In figures 11 and 12, the cylinder

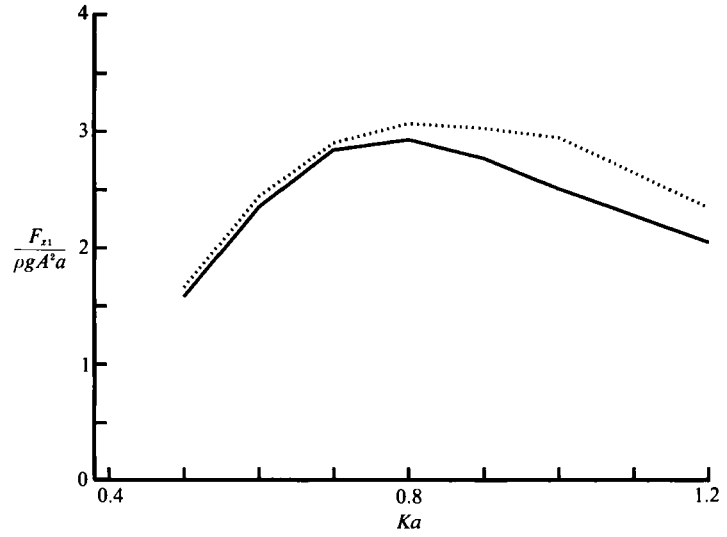

FIGURE 12. Wave drift damping coefficient for a restrained floating cylinder of radius a and draught $3a$ in head waves, obtained by numerical differentiation of F_z at $Fr = \pm 0.0319$. Solid line, present theory, 280 panels on half-S_B, 224 panels on half-S_F; dotted line, Zhao & Faltinsen (1989, figure 15).

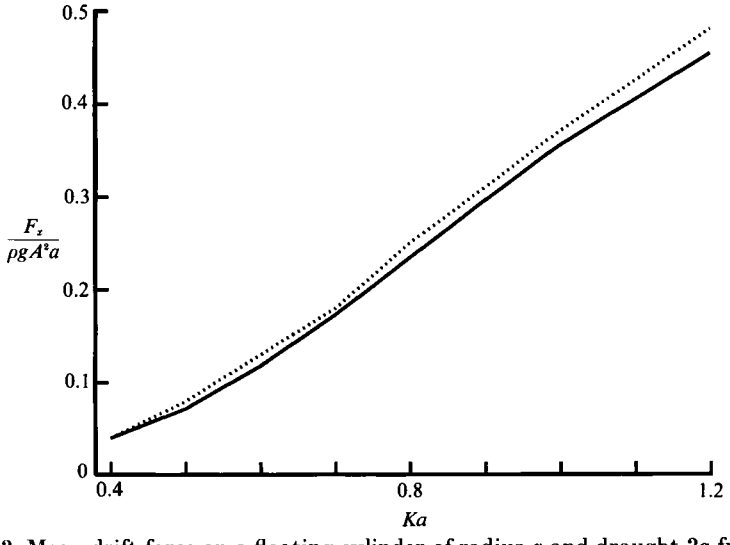

FIGURE 13. Mean drift force on a floating cylinder of radius a and draught $3a$ free to surge in head waves. $Fr = 0.0226$. Comparison between the present method (solid line) and Faltinsen (1990, p. 163) (dotted line). Present method, 280 panels on half-S_B, 224 panels on half-S_F.

is restrained, while in 13 and 14 the cylinder is free to surge. The cylinder radius is a and the draught is $3a$. The free surface is discretized out to a radius of $6a$. We have also made a comparison with results from Zhao & Faltinsen (1989) and from Faltinsen (1990), obtained with a quite different method. The results for the wave drift damping coefficient obtained from the two different methods are reasonably close.

In the figures displayed we have stopped the calculations at $Ka = 1.2$. A finer panellization of the bodies is needed for higher wavenumbers.

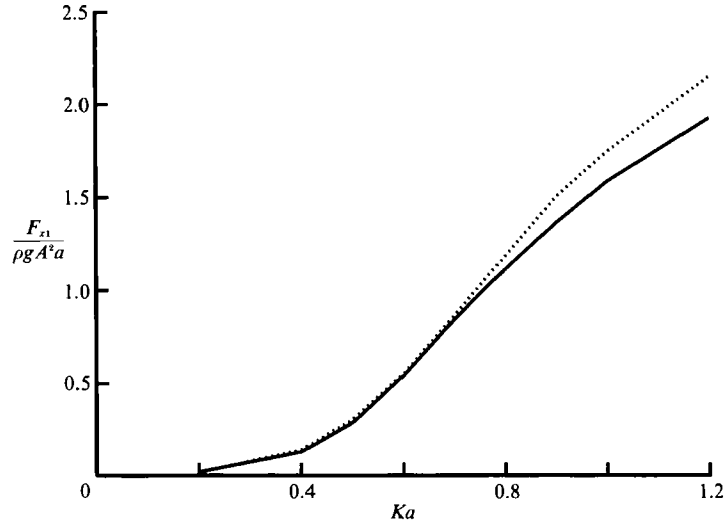

FIGURE 14. Wave drift damping coefficient for a floating cylinder of radius a and draught $3a$ free to surge in head waves, obtained by numerical differentiation of F_x at $Fr = \pm 0.0226$. Comparison between the present method (solid line) and Faltinsen (1990, p. 163) (dotted line). Present method, 280 panels on half-S_B, 224 panels on half-S_F.

6. Accuracy of the method

6.1. *The energy equation*

The energy equation relates the mean outflux of wave energy at a control surface enclosing the body to the mean work done by the pressure forces acting on the body. For the diffraction problem or the case where the body is freely floating in the waves (and there are no dissipative forces), the mean work done by the pressure forces at the body is zero. Thus, the energy flux at the control surface should be zero in this case, giving a check for the accuracy of the method. The mean energy flux through the control surface S_∞ at infinity is given by

$$W = \overline{\iint_{S_\infty} (p + \tfrac{1}{2}\rho|\boldsymbol{v}|^2 + \rho g z)\, \boldsymbol{v}\cdot\boldsymbol{n}\, \mathrm{d}S}. \tag{73}$$

Applying conservation of mass and the Bernoulli equation for the pressure we have

$$W = -\rho \iint_{S_\infty} \overline{\Phi_t \boldsymbol{v}'\cdot\boldsymbol{n}}\, \mathrm{d}S + \rho U \int_{C_\infty} \overline{\Phi_t \zeta n_1} R\, \mathrm{d}\theta, \tag{74}$$

where ζ is the free-surface elevation. We note that W is entirely determined by products of first-order quantities only. Inserting expressions (6) for ϕ_0 and (16) for the radiation and scattering potentials ϕ_j, taking the average with respect to time, and using the method of stationary phase, we obtain

$$\frac{W}{2Ec_g} = \frac{\sigma}{\omega}\left\{ \int_0^{2\pi} A(\theta)\, |H(\theta)|^2\, \mathrm{d}\theta + (1 - 2\tau\cos\beta) S \right\} + o(\tau), \tag{75}$$

where

$$A(\theta) = \tfrac{1}{2}(1 - 2\tau\cos\theta); \tag{76}$$

$E \equiv \frac{1}{2}\rho g A^2$ and c_g denote the mean energy density and the group velocity, respectively, of the incoming waves. $H(\theta)$ is given by (70) and S is given by (69).

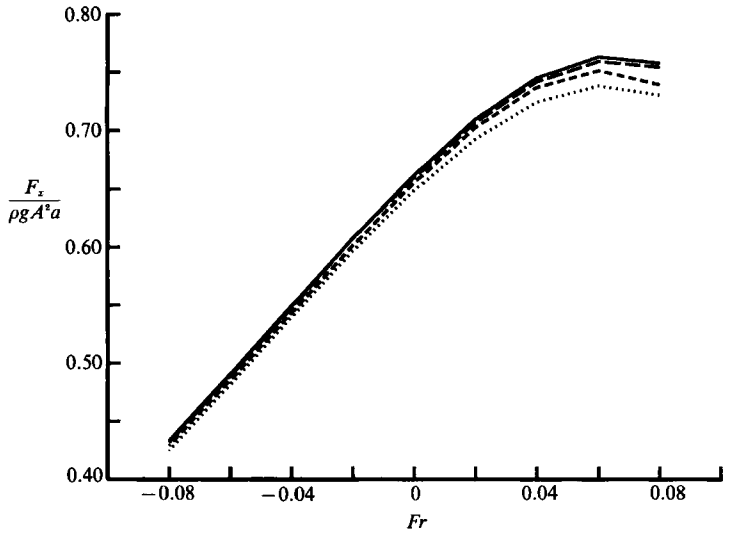

FIGURE 15. Convergence of the wave drift force for a restrained vertical cylinder. Incoming waves with $\beta = \pi$, $Ka = 1$. Number of panels on the half of S_B and on the half of S_F, respectively, are: Solid line, 416 (S_B), 228 (S_F); long-dashed line, 216 (S_B), 156 (S_F); short-dashed line, 96 (S_B), 72 (S_F); dotted line, 54 (S_B), 36 (S_F).

Fr	τ	$W/2aEc_g$	$W'/2aEc_g$
0.00	0.0000	−0.000721	−0.000721
0.02	0.0204	0.008731	0.001171
0.04	0.0416	0.029872	−0.000140
0.06	0.0636	0.065699	−0.001400
0.08	0.0864	0.118346	−0.000180

TABLE 1. Energy flux at infinity for a restrained vertical surface-piercing cylinder, with radius a and draught $3a$. The energy flux is non-dimensionalized with the incoming wave energy flux per cylinder diameter. Also values of $W'/2aEc_g \equiv W/2aEc_g - (19Fr^2 - 6Fr^3)$ are shown. The half-wetted body surface is panelled with 416 panels, and the half of the free surface with 288 panels.

Let us then, as an example, consider the energy flux at infinity for a restrained vertical surface-piercing cylinder moving with a small forward speed in head waves. The wavenumber is $Ka = 1$ and the Froude number is between 0 and 0.08. Values of $W/2Ec_g$, i.e. the outflux of energy at infinity divided by the energy flux of the incoming waves per cylinder diameter, are shown in table 1, column 3. For zero forward speed the table shows that the energy loss in the model is 7.2×10^{-4}. For increasing Froude number, however, there is a net outflux of energy at infinity, up to 12% of the incoming wave energy per cylinder diameter. This energy flux is partly due to numerical errors, and partly to contributions from higher-order terms in the Froude number, which are not taken into account in the model. Assuming that errors due to higher-order terms behave for small Froude number like $\alpha_1 Fr^2 + \alpha_2 Fr^3$, we apply the least-squares method to this function for the values of W given in the table. The result is that $\alpha_1 \approx 19$, $\alpha_2 \approx -6$. In table 1, column 4, we show values of

$$\frac{W'}{2aEc_g} \equiv \frac{W}{2aEc_g} - (19Fr^2 - 6Fr^3),$$

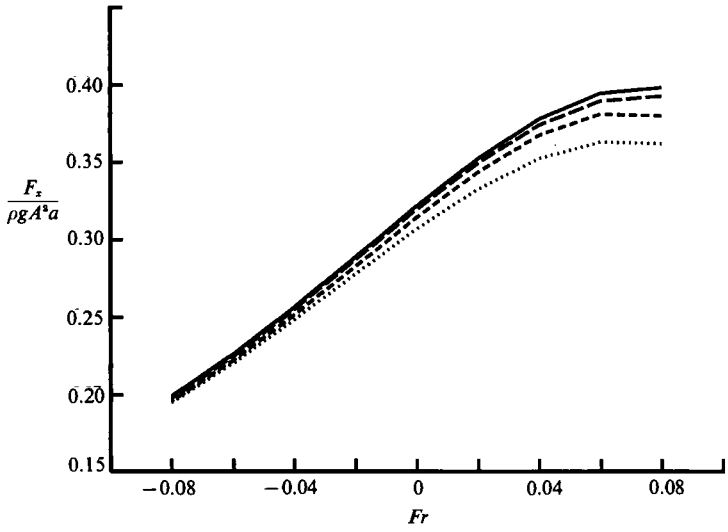

FIGURE 16. Same as figure 15, but cylinder is free to surge in linear motion.

which demonstrate that the numerical errors to first order in the Froude number are of order 10^{-3} in this case.

6.2. *Convergence of numerical method*

Let us next discuss the convergence of the numerical method for an increasing number of panels on the body surface and on the free surface. As an example, we consider the convergence of the drift force on the vertical surface-piercing cylinder, which either is restrained or free to surge in the incoming waves. The incoming waves are propagating along the negative x-axis, i.e. $\beta = \pi$, the wavenumber is $Ka = 1$, and the Froude number is between -0.08 and 0.08. In figures 15 and 16 are shown results for F_x with the number of panels on half of the wetted body surface varying from 54 to 416, and the number of panels on half of the free surface varying from 36 to 288. The figures exhibit a remarkably quick convergence of the drift force for negative values of the Froude number, while the convergence is rather slow for $Fr > 0.04$. However, the results for the finest and next finest discretizations are always very close. For these two discretizations the difference is less than 0.5 % for the restrained cylinder, while it is less than 1.5 % for the cylinder free to surge.

The figures also show a quick convergence of the wave drift damping coefficient, i.e. $(\partial F_x/\partial Fr)|_{Fr=0}$. The difference in the wave drift damping coefficient obtained by the finest and next finest discretization is less than 1 % for the restrained cylinder, and less than 2 % for the cylinder free to surge. A rough estimate of the wave drift damping coefficient, within 10 % accuracy, may even be obtained with the coarsest panellization of the cylinder. Thus, these examples demonstrate that the wave drift damping coefficient is predicted with the same accuracy as the mean drift force at zero speed.

7. Conclusion

Using a boundary-element method we have developed a numerical code which computes the velocity potential, and the first-order and mean second-order wave forces on floating bodies with small forward speed in three dimensions. From the

mean second-order force the wave drift damping coefficient is readily obtained. The method is very effective since the unknowns are located only on the wetted part of the floating body. The usual waterline integral disappears in the integral equations.

It is shown that the wave exciting forces and the mean drift forces are most influenced by a small forward velocity. The Timman–Newman relations are proved also to be valid when the steady double-body flow around the body, the χ-field, is included in the free-surface condition. From these relations it follows that the diagonal terms for added mass and damping are dependent on the forward velocity only through the frequency of encounter.

From the examples discussed we find that the energy is conserved in the model, within a very good accuracy, to first order in the forward velocity. Also, the numerical method predicts the wave drift damping coefficient with the same accuracy as the wave drift force at zero speed. Furthermore, a good estimate of the wave drift damping coefficient may be obtained with a rather coarse discretization of the body, which is of great advantage for large bodies of complicated shape. On the free surface, integration out to a distance of about 2–3 diameters from the body is sufficient. For simple bodies the wave drift damping is found to be positive. However, for complex bodies, where resonance may occur, the wave drift damping may become negative in narrow wavenumber regions, and lead to negative damping. The applicability of the so-called wave drift gradient approach is also discussed, with the conclusion that this method predicts the wave drift damping coefficient fairly well in some cases, but fails completely in other cases.

Financial support for this work has been granted by the Royal Norwegian Council for Science and the Humanities (NAVF) and by Saga Petroleum A/S. The WAMIT radiation/diffraction program has been provided by Veritas Sesam Systems A/S.

REFERENCES

FALTINSEN, O. M. 1990 *Sea Loads on Ships and Offshore Structures*. Cambridge University Press.

GRUE, J. & PALM, E. 1990 Mean forces on floating bodies in waves and current. *Proc. 5th Intl Workshop on Water Waves and Floating Bodies, Manchester, U.K.*

HASKIND, M. D. 1946 The hydrodynamic theory of ships oscillating in rolling and pitching. *Prikl. Mat. Mekh.* **10**, 33–66.

HUIJSMANS, R. H. M. & HERMANS, A. J. 1985 A fast algorithm for computation of 3-D ship motions at moderate forward speed. *4th Intl Conf. on Numerical Ship Hydrodynamics.*

MARUO, H. 1960 Wave resistance of a ship in regular head sea. *Bulletin of the Faculty of Engineering, Yokohama National University*, vol. 9.

NEWMAN, J. N. 1959 The damping and wave resistance of a pitching and heaving ship. *J. Ship Res.* **3**, 1–19.

NEWMAN, J. N. 1977 *Marine Hydrodynamics*. The MIT Press.

NEWMAN, J. N. 1978 The theory of ship motions. *Adv. Appl. Mech.* **18**, 221–280.

NEWMAN, J. N. 1984 An expansion of the oscillatory source potential. *Appl. Ocean Res.* **6**, 116–117.

NEWMAN, J. N. & SCLAVOUNOS, P. D. 1987 *WAMIT User's Manual*. MIT.

OGILVIE, T. F. & TUCK, E. O. 1969 A rational strip theory of ship motions: part 1. *Rep.* 013. The Department of Naval Architecture and Marine Engineering, The University of Michigan, College of Engineering.

SCHELLIN, T. E. & KIRSCH, A. 1989 Low-frequency damping of a moored semisubmersible obtained from simulated extinction tests and mean wave drift forces. *Appl. Ocean Res.* **11**, 202–211.

TIMMAN, R. & NEWMAN, J. N. 1962 The coupled damping coefficients of a symmetric ship. *J. Ship Res.* **5**, 1–7.

WICHERS, J. E. W. & HUIJSMANS, R. H. M. 1984 On the low frequency hydrodynamic damping forces acting on offshore moored vessels. *Proc. Offshore Technology Conf., Houston, OTC 4831.*

WICHERS, J. E. W. & SLUIJS, M. F. 1979 The influence of waves on the low frequency hydrodynamic coefficients of moored vessels. *Proc. Offshore Technology Conf., Houston, OTC 3625.*

WU, G. X. & EATOCK-TAYLOR, R. 1990 The hydrodynamic force on an oscillating ship with low forward speed. *J. Fluid Mech.* **211**, 333–353.

ZHAO, R. & FALTINSEN, O. M. 1988 Interaction between waves and current on a 2-D body in the free surface. *Appl. Ocean Res.* **10**, 87–99.

ZHAO, R. & FALTINSEN, O. M. 1989 Interaction between current, waves and marine structures. *5th Intl Conf. on Numerical Ship Hydrodynamics.*

ZHAO, R., FALTINSEN, O. M., KROKSTAD, J. R. & AANESLAND, V. 1988 Wave-current interaction effects on large-volume structures. *Proc. Intl Conf. on the Behaviour of Offshore Structures* (ed. T. Moan, N. Janbu & O. Faltinsen), vol. 2, pp. 623–638. Trondheim: Tapir Publishers.